

On the unlocking of color and flavor in color-superconducting quark matter

D. Nickel,^{1,2} R. Alkofer,² and J. Wambach^{1,3}

¹*Institute for Nuclear Physics, Technical University Darmstadt,
Schloßgartenstraße 9, D-64289 Darmstadt, Germany*

²*Institute of Physics, University of Graz, Universitätsplatz 5, A-8010 Graz, Austria*

³*Gesellschaft für Schwerionenforschung mbH, Planckstraße 1, D-64291 Darmstadt, Germany*

(Dated: 14th September 2017)

The role of the strange quark mass for the phase structure of QCD at non-vanishing densities is studied by employing a recently developed self-consistent truncation scheme for the Dyson-Schwinger equations of the quark propagators in Landau gauge. Hereby the medium modification of the effective quark interaction by the polarization of gluons is implemented. Taking into account this effect results in significantly smaller dynamical quark masses at the Fermi surface. Due to this reduction the color-flavor locked phase is always the preferred color-superconducting phase at zero temperature and for a realistic strange quark mass.

I. INTRODUCTION

The possible occurrence of different phases in Quantum Chromo Dynamics (QCD) at sufficiently high densities and small temperatures has attracted a lot of interest in recent years (for corresponding reviews see *e.g.* refs. [1, 2]). Within models, and depending on various parameters and constraints, a surprisingly rich structure of different color-superconducting phases has been studied. The pairing pattern of quarks strongly depends on the relative position of the Fermi surfaces of the different quark species. Therefore the dynamically generated constituent masses as well as the effective chemical potentials are the relevant quantities for a study of color-flavor unlocking.

The color-flavor locked (CFL) phase is expected to be the ground state for a three flavor color-superconductor at asymptotically large densities [3]. This raises the question of what happens to this state when the density is lowered to more realistic values. Since the CFL phase is neutral for degenerate quarks this depends mainly on the mass splitting between the strange quark and the two light (up and down) quarks. The unlocking of color and flavor has been investigated within models of the Nambu & Jona-Lasinio (NJL) type by varying the strange quark mass [4, 5]. It has been concluded that at some densities the CFL phase is disfavored compared to the 2-flavor color superconductor (2SC) phase in a self-consistent treatment [6]. The region of the 2SC phase possesses a rich (sub-)structure if furthermore neutrality conditions and β -equilibrium are taken into account [7]. The CFL phase and the boundary for unlocking are, however, only mildly affected.

These results, obtained in NJL-type models, are rather sensitive to model parameters. For more reliable statements a non-perturbative approach, which is directly based on the QCD degrees of freedom and recovers the correct vacuum results as well as the proper weak coupling behavior at asymptotically large densities, is needed.

For the description of QCD vacuum properties, truncated Dyson-Schwinger equations (DSEs) in Landau gauge have been successfully applied (for corresponding reviews see refs. [8]). They naturally describe gluon [9] as well as quark [10] confinement. They have furthermore been extended to non-vanishing chemical potentials with the correct behavior in the weak coupling limit [11]. Therefore this method will be employed here for the investigation of the color-flavor unlocking. Within this framework, we present self-consistent solutions of the quark propagators in the 2SC and CFL phase for realistic values of the strange-quark current mass. We include energy- and momentum-dependent dressing functions for the most general parameterization in both Dirac and color-flavor space. For the reasons stated above, we neglect for the time being the neutrality conditions in the present investigation of color-flavor unlocking. In contrast to studies employing NJL-type models, we have also implemented a medium modification of the effective quark interaction taking into account the medium contribution to the polarization tensor which enters the gluon propagator. It has to be noted that a proper description of the weak coupling limit requires the inclusion of this effect. The vacuum part of the effective quark interaction is taken either from a solution of coupled gluon, ghost and quark propagator DSEs or from a fit to lattice data for the gluon and the quark propagators [12, 13].

In the chiral limit and at moderate values of the quark density, the gap functions at the Fermi surface in such a calculation acquire sizeable values [11], comparable to those obtained within NJL-type models. These results are found to be rather insensitive to the effective quark interaction, at least within the range of uncertainty of the effective coupling. The dynamically generated mass functions, on the other hand, turn out to be significantly smaller than in the vacuum. This is due to the medium modification of the interaction (which is usually neglected in NJL-type investigations). This effect of smaller dynamical quark masses implies that the Fermi surfaces of the quarks are closer to each other than expected and eventually leads to the most important result presented here: the CFL phase is, at zero temperature and realistic values for the strange quark current mass, always energetically preferred compared to

the 2SC phase.

This paper is organized as follows: In section II we briefly present the employed theoretical framework, leading to a fully self-consistent treatment of the CFL phase for a range of strange quark masses. A physical interpretation of the parameterization used is provided. In section III we discuss the numerical results including those for Fermi momenta, mass and gap functions, etc.. Most importantly, we provide a prediction for the critical value for the strange quark current mass as a function of the chemical potential. Finally, we summarize and conclude in section IV. The color-flavor basis employed is given in the Appendix.

II. THE LANDAU-GAUGE QUARK PROPAGATOR AT NON-VANISHING CHEMICAL POTENTIAL

A. The truncated quark DSE at non-vanishing chemical potential

In ref. [11], a closed truncated DSE for the Landau-gauge quark propagator at non-vanishing chemical potential has been derived and solved in the chiral limit. In this work we are following the scheme and notations presented there. In the Nambu-Gor'kov basis (see ref. [2] for a corresponding review) the normal quark DSE is coupled to an equation for the gap functions. To describe their structure we define

$$\mathcal{S}_0(p) = \begin{pmatrix} S_0^+(p) & 0 \\ 0 & S_0^-(p) = -CS_0^+(-p)^TC \end{pmatrix}, \quad (1)$$

$$\mathcal{S}(p) = \begin{pmatrix} S^+(p) & T^-(p) = \gamma_4 T^+(p)^\dagger \gamma_4 \\ T^+(p) & S^-(p) = -CS^+(-p)^TC \end{pmatrix}, \quad (2)$$

$$\Sigma(p) = \begin{pmatrix} \Sigma^+(p) & \Phi^-(p) \\ \Phi^+(p) & \Sigma^-(p) \end{pmatrix}, \quad (3)$$

with \mathcal{S}_0 being the bare and \mathcal{S} the full Nambu-Gor'kov propagator. Σ is the Nambu-Gor'kov self-energy. S_0^+ is diagonal in color-flavor space and equal to $S_{0,f}^+(p)^{-1} = -i(p_4 + i\mu)\gamma_4 - i\vec{p}\cdot\vec{\gamma} + m_{0,f}$ for a quark flavor f . As the Euclidean action is real we furthermore have to impose $\Phi^-(p) = \gamma_4 \Phi^+(p)^\dagger \gamma_4$. Introducing appropriate renormalization constants, the DSE for the quark propagator

$$\mathcal{S}^{-1}(p) = Z_2 \mathcal{S}_0^{-1}(p) + Z_{1F} \Sigma(p) \quad (4)$$

explicitly leads to

$$T^\pm = -Z_{1F} \left(Z_2 S_0^\mp^{-1} + Z_{1F} \Sigma^\mp \right)^{-1} \Phi^\pm S^\pm, \quad (5)$$

$$S^{\pm-1} = Z_2 S_0^{\pm-1} + Z_{1F} \Sigma^\pm - Z_{1F}^2 \Phi^\mp \left(Z_2 S_0^\mp^{-1} + Z_{1F} \Sigma^\mp \right)^{-1} \Phi^\pm. \quad (6)$$

Employing the truncation of ref. [11], the equations for the self-energy and the gap function then read

$$\Sigma^+(p) = \frac{Z_2^2}{Z_{1F}} \pi \int \frac{d^4 q}{(2\pi)^4} \gamma_\mu \lambda_a S^+(q) \gamma_\nu \lambda_a \left(\frac{\alpha_s(k^2) P_{\mu\nu}^T}{k^2 + G(k)} + \frac{\alpha_s(k^2) P_{\mu\nu}^L}{k^2 + F(k)} \right), \quad (7)$$

$$\Phi^+(p) = -\frac{Z_2^2}{Z_{1F}} \pi \int \frac{d^4 q}{(2\pi)^4} \gamma_\mu \lambda_a^T T^+(q) \gamma_\nu \lambda_a \left(\frac{\alpha_s(k^2) P_{\mu\nu}^T}{k^2 + G(k)} + \frac{\alpha_s(k^2) P_{\mu\nu}^L}{k^2 + F(k)} \right), \quad (8)$$

where $k = p - q$. Here projectors transverse and longitudinal in the medium have been introduced. The functions G and F describe the corresponding medium modifications of the gluon propagator, see Eq. (21) of ref. [11] and are calculated, once the coupling is given. Therefore the only input for the quark DSE are the running coupling $\alpha_s(k^2)$ (for its choice see below) and the renormalized quark current masses.

Before proceeding we note that this quark DSE can also be derived from the thermodynamically consistent effective action corresponding to the truncation scheme used [11]. Evaluating this action at the stationary point one obtains:

$$\begin{aligned} \Gamma[\mathcal{S}] &= -\frac{1}{2} \text{Tr}_{p,D,c,f,NG} \text{Ln} \mathcal{S}^{-1} + \frac{1}{4} \text{Tr}_{p,D,c,f,NG} (1 - Z_2 \mathcal{S}_0^{-1} \mathcal{S}) + \text{const.} \\ &= -\frac{1}{2} \text{Tr}_{p,D,c,f} \text{Ln} \left(S^{+-1} (Z_2 S_0^{-1} + Z_{1F} \Sigma^-) \right) + \\ &\quad + \frac{1}{4} \text{Tr}_{p,D,c,f} (2 - Z_2 S^+ S_0^{+-1} - Z_2 S^- S_0^{-1}) + \text{const.} \end{aligned} \quad (9)$$

Later on we will use this expression to determine *e.g.* the pressure difference between different phases at a given chemical potential.

Similar to our previous investigation in the chiral limit [11], we employ two different couplings. The running coupling determined in DSE studies of the Yang-Mills sector [12], which is labeled in the following as $\alpha_I(k^2)$, will serve as a lower bound. As is detailed in ref. [12] it underestimates chiral symmetry breaking significantly in the abelian approximation, which on the other hand is an appropriate choice if the ground state does not break chiral symmetry dynamically or explicitly, see ref. [10] and references therein. The running coupling extracted from lattice QCD data for the quark and gluon propagators [13] will serve as an upper bound, since the medium will probably weaken the interaction. It is labeled $\alpha_{II}(k^2)$. In order to vary the renormalization point in the latter version of the coupling, we use the multiplicative renormalizability of the quark DSE. Note also that the vacuum quark propagator, determined within such a scheme [14] is in excellent agreement with the corresponding lattice data when the finite volume of lattice calculations is accounted for.

As stated above, taking into account the medium polarization, Debye screening and Landau damping are included. Both, screening and damping of the interaction increase for increasing interaction strength. Therefore the generated gap and mass (normal self-energy) functions turn out to be much less sensitive against variation of $\alpha_s(k^2)$ than the dynamical mass function in the chirally broken vacuum. Due to this fortunate instance the presented approach has considerable predictive power despite the uncertainty in the effective low-energy quark interaction at non-vanishing densities.

The renormalization constants are determined in the (chirally broken) vacuum. Due to the employed vertex construction, the quark-gluon vertex renormalization constant, Z_{1F} , cancels in the resulting renormalized equations. For each flavor, we determine the quark wave-function renormalization constant, Z_2 , and the renormalization constant Z_m , relating the unrenormalized quark mass $m_{0,q}(\Lambda^2)$ at an ultraviolet cutoff Λ to the renormalized mass $m_q(\nu)$ via

$$m_{0,q}(\Lambda^2) = Z_m(\nu^2, \Lambda^2)m_q(\nu), \quad (10)$$

by requiring

$$S_q^+(p)|_{p^2=\nu^2} = -i\not{p} + m_q(\nu) \quad (11)$$

at a renormalization scale ν . This corresponds to a momentum-subtraction (*MOM*) scheme, which results in somewhat smaller numerical values for the quark current masses at a given renormalization scale (usually taken to be 2 GeV). We simply ignore here the difference between \overline{MS} and *MOM* masses because the effect is of the order of ten percent (when calculated within perturbation theory) and thus much smaller than the uncertainty in the value the current masses [20].

It turns out that, as expected, the mass dependence of the quark wave function renormalization constant, Z_2 , is negligible as long as the renormalization scale is much larger than the mass. Therefore, we simply drop this dependence and Z_2 is determined once and for all in the chiral limit. To keep the number of parameters as small as possible, we work in the chiral isospin limit (*i.e.* we set the up and down current quark masses to zero) and vary only the strange quark current mass.

In the following we will restrict to isotropic phases. In order to solve the DSE of the quark propagator it is advantageous to consider their color-flavor structure first. To get a self-consistent solution we choose suitable sets of matrices $\{P_i\}$ and $\{M_i\}$ in color-flavor space, such that

$$\Sigma^+(p) = \frac{Z_2}{Z_{1F}} \sum_i \Sigma_i^+(p) P_i, \quad (12)$$

$$\Phi^+(p) = \frac{Z_2}{Z_{1F}} \sum_i \phi_i^+(p) M_i, \quad (13)$$

where we have introduced the renormalization-point independent component functions $\Sigma_i^+(p)$ and $\phi_i^+(p)$, which are matrix-valued in Dirac space. Full self-consistency is guaranteed in case a basis of all allowed matrices is considered. The dimensionality of this basis in a given phase depends on the residual symmetry in color-flavor space. For the CFL phase this will be detailed below.

The Dirac structure of the self-energies in an even-parity phase can be parameterized by [16]

$$\Sigma_i^+(p) = -i\not{p} \Sigma_{A,i}^+(p) - i\phi_p \Sigma_{C,i}^+(p) + \Sigma_{B,i}^+(p) - i\gamma_4 \not{p} \Sigma_{D,i}^+(p), \quad (14)$$

$$\phi_i^+(p) = \left(\gamma_4 \not{p} \phi_{A,i}^+(p) + \gamma_4 \phi_{B,i}^+(p) + \phi_{C,i}^+(p) + \not{p} \phi_{D,i}^+(p) \right) \gamma_5, \quad (15)$$

where $\hat{p} = \vec{p}/|\vec{p}|$, $\not{p} = \hat{p} \cdot \vec{\gamma}$, $\phi_p = \omega_p \gamma_4$ and $\omega_p = ip_4 + \mu$. We already note that $\Sigma_{D,i}^+(p)$ turns out to be negligibly small. This is to be expected since it has to vanish due to time reversal symmetry at vanishing temperatures in color-flavor

symmetric channels. The gap functions ϕ_B and ϕ_D , which vanish in the chiral limit will be discussed in subsection II C where we provide an interpretation in a simplified setting.

The system of equations for the self-energies is symmetric under the transformations

$$\Sigma_{A/B/C,i}^+(p_4, |\vec{p}|) \rightarrow \Sigma_{A/B/C,i}^+(-p_4, |\vec{p}|)^*, \quad (16)$$

$$\Sigma_{D,i}^+(p_4, |\vec{p}|) \rightarrow -\Sigma_{D,i}^+(-p_4, |\vec{p}|)^*, \quad (17)$$

which we find to be unbroken in the self-consistent scheme presented here. Therefore, the determinant of the quark propagator is positive for $p_4 = 0$, and the Luttinger theorem is applicable for determining the density [11].

For the anomalous propagator an inhomogeneous part is missing in Eq.(5). Therefore we can choose a global phase for the gap functions. This is done such that the equations are invariant under

$$\phi_{A/D,i}^+(p_4, |\vec{p}|) \rightarrow \phi_{A/D,i}^+(-p_4, |\vec{p}|)^* \quad (18)$$

$$\phi_{B/C,i}^+(p_4, |\vec{p}|) \rightarrow -\phi_{B/C,i}^+(-p_4, |\vec{p}|)^*, \quad (19)$$

and therefore ϕ_A and ϕ_D are real, and ϕ_B and ϕ_C purely imaginary, for $p_4 = 0$.

Neglecting $\Sigma_{D,i}^+$, the Dirac structure of the inverse normal propagator can be written as

$$S_i^{+-1}(p) = Z_2 S_{0,i}^{+-1} + Z_{1F} \Sigma_i^+ = -i\vec{p} \cdot \vec{A}_i(p) - i\psi_p C_i(p) + B_i(p), \quad (20)$$

which allows to define the mass function for the pairing quasiparticles for a given color-flavor channel q as

$$M_q(p) = \frac{m_{0,q} + \Sigma_{B,q}^+(p)}{1 + \Sigma_{C,q}^+(p)}. \quad (21)$$

In the following we will mostly present results for mass functions at $p_4 = 0$. To ease notations we will use $M_q(|\vec{p}|) = M_q(p_4 = 0, |\vec{p}|)$ except when stated explicitly otherwise.

B. The parameterization of the CFL phase

As its name already expresses, the CFL phase is defined via its symmetry pattern in color-flavor space. For three degenerate quark flavors, one considers the $SU(3)_{c+V}$ symmetry generated by $\tau_a - \lambda_a^T$, with $a = 1, \dots, 8$ and τ_a, λ_a being the Gell-Mann matrices in flavor and color space, respectively [3]. The quarks therefore are in a $\mathbf{3} \otimes \bar{\mathbf{3}} = \mathbf{1} \oplus \mathbf{8}$ representation of this symmetry. In the case of only two degenerate quarks and a strange quark, the symmetry is broken down to $SU(2)_{c+V} \otimes U(1)_{c+V}$, which is generated by $\tau_a - \lambda_a^T$ with $a = 1, 2, 3$ and 8, *i.e.* the quarks form a $\mathbf{1} \oplus \mathbf{1} \oplus \mathbf{2} \oplus \mathbf{2} \oplus \mathbf{3}$ representation.

For the Nambu-Gor'kov propagator to be invariant under this transformation, we need to require

$$U^\dagger S^+(p) U = S^+(p), \quad U^T T^+(p) U = T^+(p), \quad (22)$$

for $U \in SU(2)_{c+V} \otimes U(1)_{c+V}$. The matrices $\{P_i\}$ and $\{M_i\}$, needed for a self-consistent description are then those given explicitly in the Appendix.

In section III we will also present results for the self-energies evaluated at different energies and momenta, in particular at the Fermi surface. In contrast to the chiral limit, where the matrices $\{P_i\}$ can be chosen as constant projectors onto irreducible representations of the residual symmetry, the situation is more complex here. In principle, every dressing function of the normal propagator and self-energy can be decomposed into irreducible projectors in color-flavor space:

$$F = F_1 P_1 + F_{1'} P_{1'} + F_2 P_2 + F_{\bar{2}} P_{\bar{2}} + F_3 P_3, \quad (23)$$

where, in particular, $P_2 = P_7$, $P_{\bar{2}} = P_8$ and $P_3 = P_1 - \frac{1}{2} P_2$. However, for every dressing function, the singlets are not protected against mixing and therefore their projectors P_1 and $P_{1'}$ are in general energy and momentum dependent. We therefore find six different Fermi momenta, which are defined as sign changes of the determinant of the propagator, $\det(\mathcal{S}(p_4 = 0, |\vec{p}|))$, at $p_4 = 0$ and connected to the density by the Luttinger theorem. Three of them correspond to the upper 3×3 block-matrix in the ansatz employed (see Appendix) and describe the mixing of the two singlet channels as well as the triplet channel. After ordering, these are denoted by $p_{F,1}$, $p_{F,1_2}$ and $p_{F,1_3}$. In the lower 6×6 diagonal block-matrix, we find $p_{F,2}$, $p_{F,\bar{2}}$ and $p_{F,3}$ corresponding to P_7 , P_8 and P_6 , respectively.

For the dressing functions of the anomalous propagators and the gap functions the situation is similar. With $M = \lambda_2 \otimes \tau_2 + \lambda_5 \otimes \tau_5 + \lambda_7 \otimes \tau_7$ being invertible and fulfilling $U^T M U = M$, we define $M_i = M P_i$. Every dressing function can then be written as

$$G = G_1 M_1 + G_1' M_1' + G_2 M_2 + G_2' M_2' + G_3 M_3, \quad (24)$$

where $M_2 = M_7$, $M_2' = M_8$ and $M_3 = M_1 - \frac{1}{2} M_2$. Furthermore M_1 and M_1' are again in general energy and momentum dependent due to the possible mixing between the singlets.

C. The gap functions ϕ_B and ϕ_D

Having introduced the most general Dirac structure for the gap functions in an even-parity phase (see Eq.(15)) their interpretation and in particular their relation to the energy gap in the excitation spectrum is of interest. To this end one has to determine the dispersion relations as given by the poles of the propagators. This is a solvable task but leads already for degenerate quarks and constant dressing functions to very involved and intricate expressions. A physically motivated approximation with a simple interpretation of the gap function will be introduced in this subsection and will serve as an illustration. For simplicity, we consider the pairing of only two different quasiparticles a and b with inverse propagators in Dirac space, given by $S_{a/b}^{+ -1} = Z_2 S_{0,a/b}^{+ -1} + Z_2 \Sigma_{a/b}^+$ for vanishing gap functions. This is in particular the case for the three lower 2×2 block-matrices in the ansatz presented in the Appendix.

The gapped propagator S_c^+ in one channel, see Eq. (6), is then typically given by

$$S_c^{+ -1} = S_a^{+ -1} - \phi^- S_b^- \phi^+, \quad (25)$$

with ϕ^+ of the form in Eq. (15). The propagators, being of the form in Eq. (20), can be expressed via the energy-projectors for $i = a, b, c$

$$S_i^{+ -1} = \sum_{e=\pm} (-i\omega C_i - e E_i) \gamma_4 \Lambda_i^e, \quad (26)$$

where

$$\Lambda_i^\pm = \frac{1}{2} (1 \pm (i\beta_i \gamma_4 \not{p} + \alpha_i \gamma_4)), \quad (27)$$

and $E_i = \sqrt{\vec{p}^2 A_i^2 + B_i^2}$, $\alpha_i = B_i/E_i$ and $\beta_i = |\vec{p}| A_i/E_i$. Neglecting the p_4 -dependence in the dressing-functions and absorbing C_a and C_b by rescaling E_a , E_b and ϕ_i correspondingly [21], we assume that no pairing between quasiparticles and anti-quasiparticles takes place. This reduces Eq. (25) to

$$(-i\omega C_c - E_c) \gamma_4 \Lambda_c^+ \approx (-i\omega - E_a) \gamma_4 \Lambda_a^+ - \phi^- \frac{1}{-i\omega^* + E_b} \Lambda_b^- \gamma_4 \phi^+, \quad (28)$$

which is exact in the chiral limit. Note, that it can also be justified, at least in leading order, in a ϕ^2/μ^2 expansion. Evaluating the roots of the right-hand side, we find the dispersion relation

$$\begin{aligned} -ip_4 = \frac{E_a - E_b}{2} \pm \left(\left(\frac{E_a + E_b}{2} - \mu \right)^2 + \phi_A^2 - \phi_B^2 - \phi_C^2 + \phi_D^2 \right. \\ \left. + 2i\phi_C (\beta_2 \phi_A - \alpha_2 i\phi_B) - 2\phi_D (\alpha_2 \phi_A + \beta_2 i\phi_B) \right)^{\frac{1}{2}}, \end{aligned} \quad (29)$$

where we have made use of the fact that ϕ_A and ϕ_D are real and ϕ_B and ϕ_C are imaginary at $p_4 = 0$ (see the discussion in the last subsection). Noting that $\alpha_i^2 + \beta_i^2 = 1$, the above expression suggests to introduce gap functions, which are transformed accordingly:

$$\tilde{\phi}_A = \beta_2 \phi_A - \alpha_2 i\phi_B, \quad i\tilde{\phi}_B = \alpha_2 \phi_A + \beta_2 i\phi_B. \quad (30)$$

This transformation depends on the mass parameter of the quasiparticle, which makes evident that the existence of the functions ϕ_B and ϕ_D allows different energy gaps for quasiparticles with different masses. In terms of the ‘rotated’ gap functions $\tilde{\phi}_A$ and $\tilde{\phi}_B$ we obtain

$$-ip_4 = \frac{E_a - E_b}{2} \pm \left(\left(\frac{E_a + E_b}{2} - \mu \right)^2 + (\tilde{\phi}_A + i\phi_C)^2 + (\phi_D - i\tilde{\phi}_B)^2 \right)^{\frac{1}{2}}. \quad (31)$$

In analogy to the situation in the chiral limit, we arrive now at a simple interpretation: One has a chirally symmetric pairing via $\tilde{\phi}_A + i\phi_C$ and a chirality breaking pairing through $\phi_D - i\tilde{\phi}_B$. For anti-quasiparticle pairing $\tilde{\phi}_A$ and $\tilde{\phi}_B$ simply change sign. In the chiral limit we then find, as expected, $\phi^\pm = \phi_A \pm i\phi_C$ and $\phi_B = \phi_D = 0$.

III. RESULTS

As described above, the quark propagator is highly non-trivial. The Dirac structure of the self-energies and gap functions is given by four self-consistently determined functions, respectively, which are in addition functions of $|\vec{p}|$ and p_4 . In accordance with the aim of this paper, namely to investigate the phenomenological importance of the strange quark current mass, we mainly restrict ourself to the presentation of results at $p_4 = 0$ and some values of $|\vec{p}|$. This will also turn out to be sufficient to demonstrate the important differences of our results as compared to corresponding ones obtained in NJL-type models. As already mentioned, we include self-energy effects, which have been analyzed so far only in the weak coupling regime [17]. Note that in the chiral limit the dependence on $|\vec{p}|$ has already been discussed in ref. [11] and the role of a non-trivial p_4 -dependence in ref. [18].

The following results will be presented for the couplings discussed above, $\alpha_I(k^2)$ and $\alpha_{II}(k^2)$. As explained, we consider them as the limiting cases, which are allowed by the uncertainty within investigations of infrared QCD. We will see that gap functions and Fermi momenta are quite insensitive to the coupling used.

A. Fermi momenta

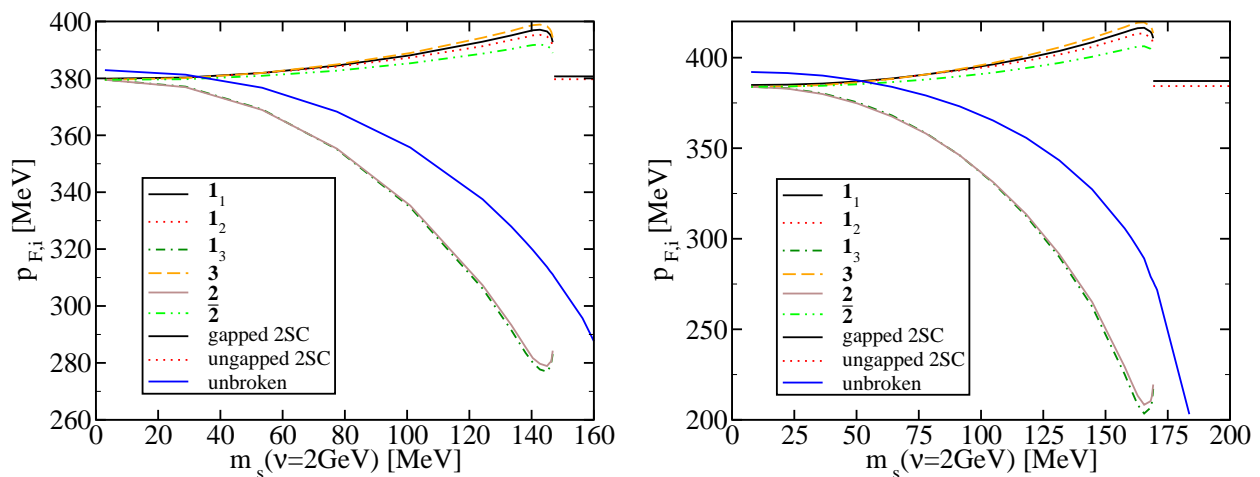


Figure 1: Fermi momenta in different channels (see text) at $\mu = 400$ MeV for the coupling $\alpha_I(k^2)$ (left) and $\alpha_{II}(k^2)$ (right).

In Fig. 1 the results for the Fermi momenta at a chemical potential of $\mu = 400$ MeV as a function of the renormalized strange quark current mass $m_s(\nu)$ at a renormalization scale $\nu = 2$ GeV are presented. For the CFL phase these are of course only plotted below the critical value of the strange quark current mass. (For the definitions of the different components see section II B.) Above this critical value the 2SC phase is energetically preferred, and the three different Fermi momenta of the 2SC phase are shown: For the gapped red and green, up- and down-quarks and the ungapped blue up- and down-quarks, which are both independent of the strange quark mass and for the decoupled strange quarks in the unbroken phase (which is also displayed below the critical of m_s).

In the CFL phase the Fermi momenta are not monotonous functions of m_s . This is due to the behavior of the vector self-energies and not visible in the mass functions, *cf.* Fig. 2.

B. Mass functions

As a function of m_s , we display in Fig. 2 the results for the constituent quark mass function in the vacuum at vanishing momenta $M_{s,broken\ vacuum}(0)$, as well as the quark mass function in the unbroken phase $M_{s,unbroken}(p_F)$ and the doublet channel in the CFL phase $M_{s,CFL-2}(p_F)$, both at their respective Fermi momenta and for a chemical potential of $\mu = 400$ MeV. Furthermore, the quark mass function in the unbroken phase $M_{s,unbroken}(2\text{ GeV})$ for the same chemical potential at the renormalization scale $\nu = 2$ GeV is given.

Although the constituent quark mass in the vacuum $M_{s,broken\ vacuum}(0)$ is very sensitive to the choice of the coupling, especially for small renormalized strange quark masses, the mass functions at finite chemical potentials are not. As explained in the previous section, this is due to the medium modification of the coupling, which also leads

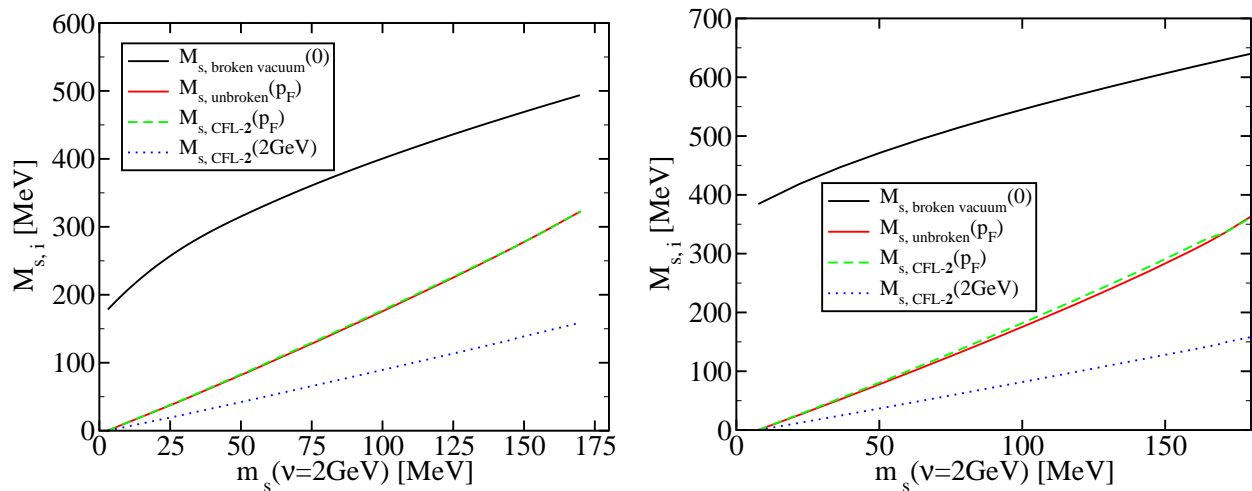


Figure 2: Mass functions at different values of three-momentum (see text) as function of the renormalized strange quark mass at a chemical potential of $\mu = 400$ MeV for the coupling $\alpha_I(k^2)$ (left) and $\alpha_{II}(k^2)$ (right).

to significantly smaller mass values at the Fermi surface. Note furthermore that the values of the mass functions at the Fermi surface in the chirally broken phase and the CFL phase are very close to each other. This leads to the conclusion that the dynamics near the Fermi surface, where gapped and ungapped propagators strongly differ, are not directly relevant for the dynamical mass generation. As expected, the mass functions at the renormalization scale are comparable to the values in the chirally broken vacuum, which confirms that ν is already sufficiently above the scale of dynamical mass generation and the Fermi energy.

C. Dependence of the gap functions on the renormalized strange-quark current mass

In this section we present results for the gap functions at the Fermi surface, *i.e.* at $p_4 = 0$, and selected values of the three-momentum. The renormalization-point independent gap functions (15) for the triplet, doublet and anti-doublet channel (*cf.* Eq. (24)) are evaluated at their corresponding Fermi momentum (see section II B). The functions $\phi_{i,1(ud)}$, $\phi_{i,1(uds)}$ and $\phi_{i,1(bs)}$, corresponding to M_2 , M_4 and M_3 , given in the Appendix, are evaluated at $(p_{F,1_1} + p_{F,1_2})/2$, $(p_{F,1_1} + p_{F,1_2} + 2p_{F,1_3})/4$ and $p_{F,1_3}$, respectively. Due to this, the functions are considered at momenta corresponding to the pairing quasiparticles. This also allows to recover the results at the Fermi surface for the CFL phase in the chiral limit. The corresponding numerical results are shown in Fig. 3 for the coupling $\alpha_I(k^2)$ and in Fig. 4 for the coupling $\alpha_{II}(k^2)$. Note again that due to the phase choice the gap functions $\phi_{A,i}$ and $\phi_{D,i}$ are real and $\phi_{B,i}$ and $\phi_{C,i}$ imaginary at $p_4 = 0$.

All functions, apart from $\phi_{i,1(bs)}$, evolve towards the corresponding 2SC solution. However, $\phi_{i,1(bs)}$ already shows that the transition must be first order. Furthermore, for the gap functions $\phi_{i,1(ud)}$ and $\phi_{i,3}$, describing non-strange pairing, ϕ_B and ϕ_D vanish, as expected. Finally, we see for the other gap functions, relevant to strange pairing, that ϕ_B is the most varying and ϕ_D is non-vanishing, which is in line with the interpretation of the gap functions given in section II C. It again is obvious that the sensitivity of the gap functions on the used coupling is much weaker than those of the mass functions.

D. Dependence of mass functions on the chemical potential

We proceed by discussing the dependence on the chemical potential and treat the case of the mass functions first. Fig. 5 shows these mass functions in the doublet channel for two different renormalized strange-quark current masses, evaluated at the Fermi momentum and at the renormalization scale, respectively.

For small enough chemical potentials, the 2SC phase is preferred and the doublet channel corresponds to decoupled strange quarks in the truncation used. Depending on the value of the renormalized strange quark mass, the strange quarks may not condense for small enough chemical potential, *i.e.* not develop a Fermi surface. This can be seen from Fig. 5 for a renormalized strange quark mass of $m_s = 200$ MeV. In this case, we evaluate the mass function at vanishing momentum and the onset of strange quark condensation is reflected as a kink in the curves. With

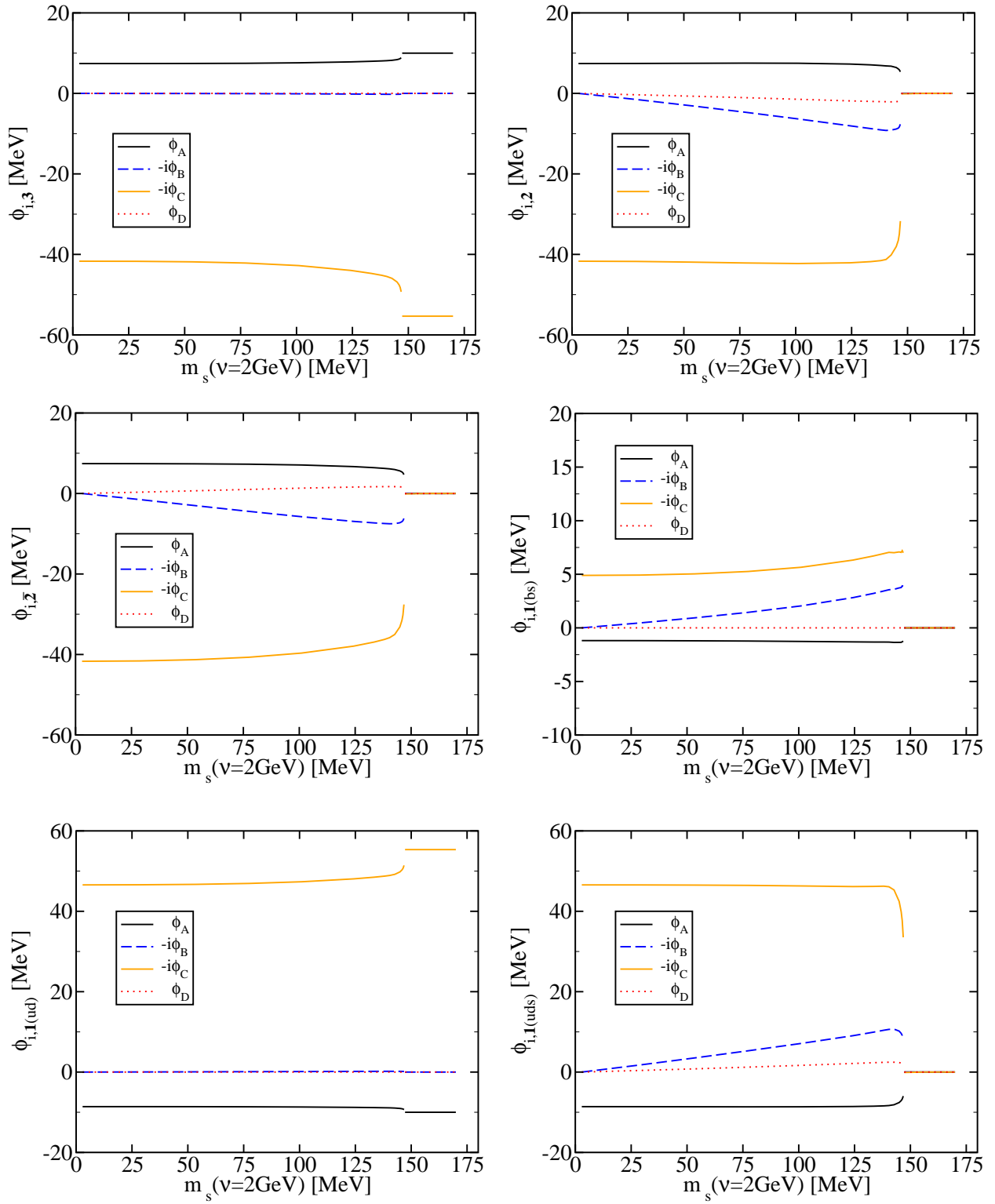


Figure 3: Gap functions at selected values of the three-momentum for different channels (see text) as a function of the renormalized strange-quark mass at a chemical potential of $\mu = 400$ MeV and for the coupling $\alpha_I(k^2)$.

rising chemical potential, the system undergoes a phase transition into the CFL phase. This effects the value of the mass function on the Fermi surface only slightly and is shown as a gap in the plots. For the coupling $\alpha_{II}(k^2)$ at $m_s = 100$ MeV we find a direct transition of non-condensed strange quarks into the CFL phase.

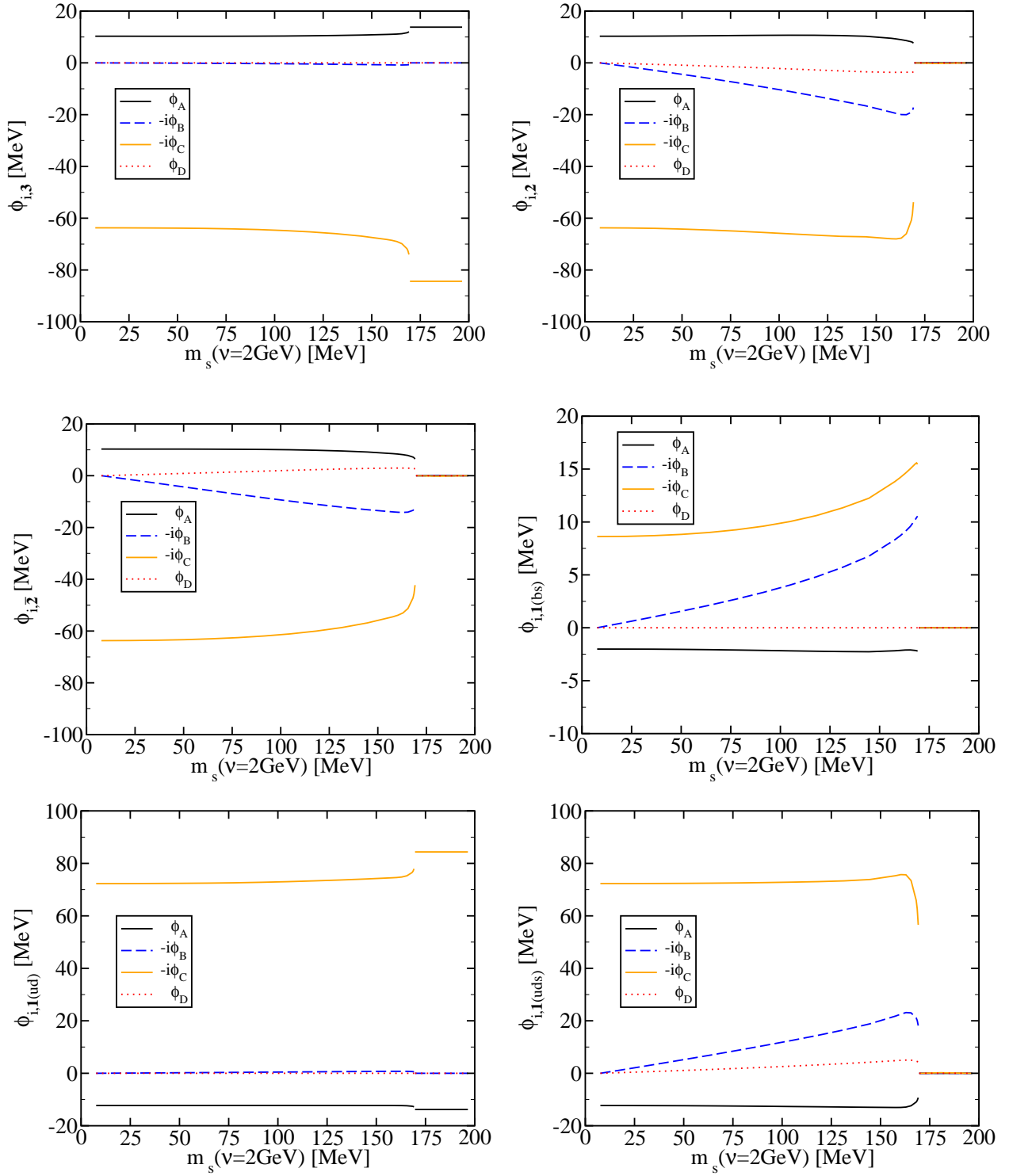


Figure 4: Gap functions at selected values of the three-momentum for different channels (see text) as function of the renormalized strange-quark mass at a chemical potential of $\mu = 400$ MeV and for the coupling $\alpha_{II}(k^2)$.

The values of the mass functions at the renormalization scale only show a slight dependence on the chemical potential and are comparable to those in the chirally broken vacuum, which again reflects the fact that the renormalization scale is well above the dynamical chiral symmetry breaking scale and the chemical potential. On the other hand, the values of the mass functions at the Fermi surface already at a chemical potential of $\mu = 1$ GeV are close to their values at the renormalization scale. As a result, dynamical chiral breaking is suppressed and the mass function is only

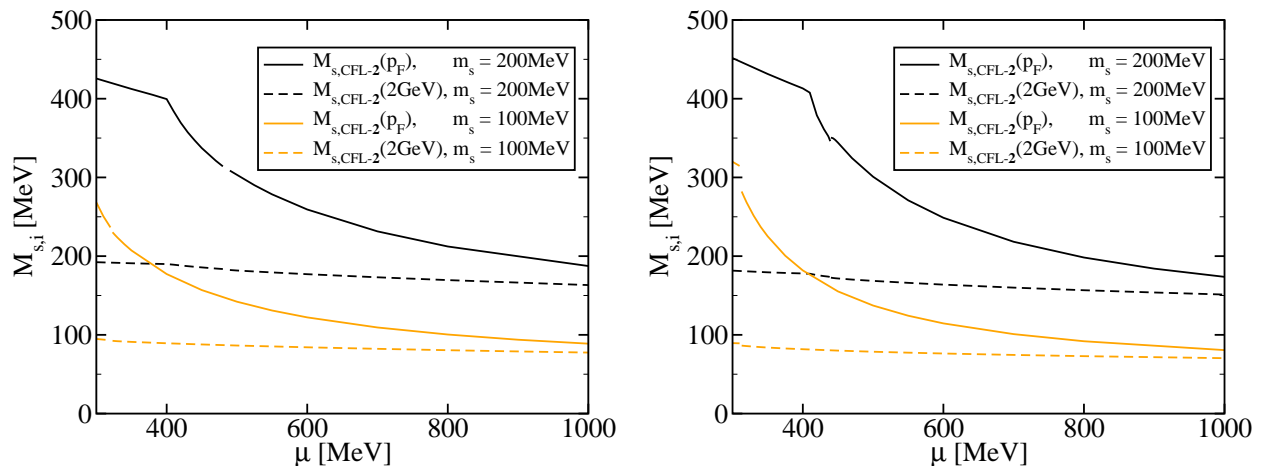


Figure 5: Mass functions on the Fermi surface and at a renormalization scale $\nu = 2$ GeV for fixed renormalized strange quark mass in the vacuum as function of the chemical potential for the coupling $\alpha_I(k^2)$ (left) and $\alpha_{II}(k^2)$ (right).

weakly dependent on the momentum below the renormalization scale.

E. Dependence of gap functions on the chemical potential

For completeness we also present results for the dependence of the gap functions on the chemical potential. In Fig. 6 we show the results for the gap functions in the CFL phase at a renormalized strange quark mass of $m_s(\nu = 2 \text{ GeV}) = 200 \text{ MeV}$ and for the coupling $\alpha_I(k^2)$. As described above, the 2SC phase is preferred for smaller chemical potentials and we find again a visible jump in the $\phi_{i,1}(ud)$ functions at a certain chemical potential. The gap functions in the CFL phase are remarkably insensitive in the chemical potential. Only the ϕ_B and ϕ_D functions evolve towards zero, which again reflects that the relevant values of the mass functions also become smaller.

F. Pressure difference and critical strange-quark mass

We now turn to the main result of this investigation: The determination of the critical value of the strange-quark current mass. Above this mass the Fermi surfaces are so far separated that pairing of up and down quarks with strange quarks is no longer energetically preferred. Based on the CJT-formalism we determine the pressure difference of CFL and 2SC using Eq. (9). The results as a function of the renormalized strange quark current mass for different chemical potentials and for the couplings employed is shown in Fig. 7. One sees, as expected, that for small masses the CFL phase is preferred, and that there is a critical value of the strange-quark mass where the CFL phase becomes energetically disfavored.

We like to emphasize that we are no longer able to find a solution for the CFL phase in case the 2SC phase becomes favored. This is considered as a consequence of the numerical method to solve the truncated DSE being the functional derivative of the truncated CJT action. It turns out that we always only find the global minimum of the CJT action as long as the local minimum is not protected by a higher symmetry. The latter is the case for the 2SC phase, if the CFL one is preferred. Nevertheless we can judge from the behavior of the gap functions that the transition is first order.

In Fig. 8 the results for the critical value of the renormalized strange-quark mass as a function of the chemical potential are given and compared to the range of the physical strange-quark current mass as determined by the particle data group [19]. (As stated above, the difference between this mass in the MOM and the \overline{MS} regularization scheme is negligible compared to the experimental uncertainty.) As can be seen, the approach taken here predicts that the physical strange-quark current mass is very likely too small for allowing a 2SC phase at zero temperature for any chemical potential. This result is remarkably stable against the variation of the running coupling $\alpha_s(k^2)$.

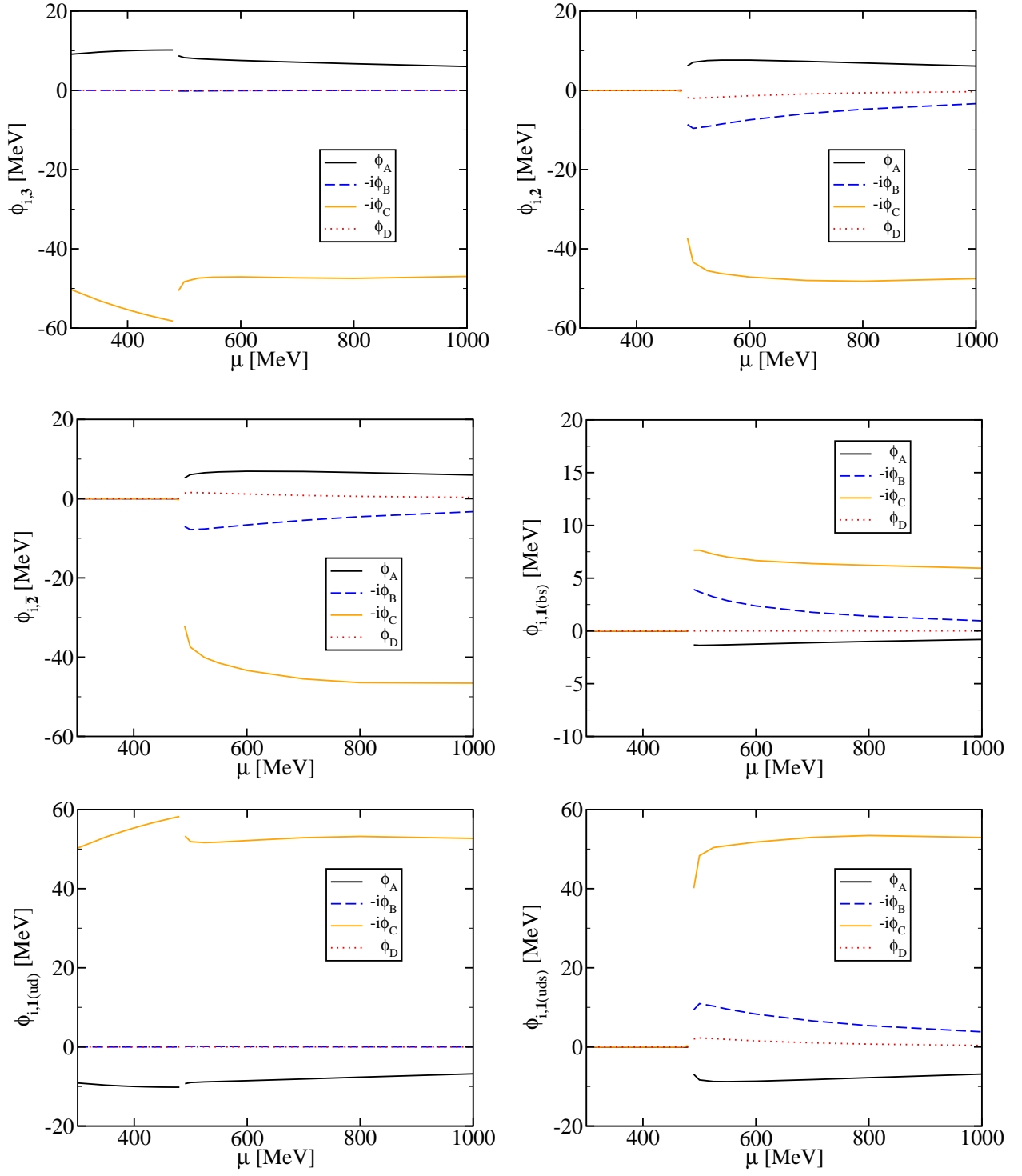


Figure 6: Gap functions on the Fermi surface for different channels (see text) at $m_s(\nu = 2 \text{ GeV}) = 200 \text{ MeV}$ as a function of chemical potential for the coupling $\alpha_I(k^2)$.

IV. CONCLUSIONS AND OUTLOOK

We have studied the quark propagator in the 2SC and CFL phase at zero temperature for different values of the strange-quark current mass in a fully self-consistent Dyson-Schwinger approach to color-superconductivity. Due to the medium modification of the interaction we find the 2SC phase to be disfavored at any physically relevant chemical

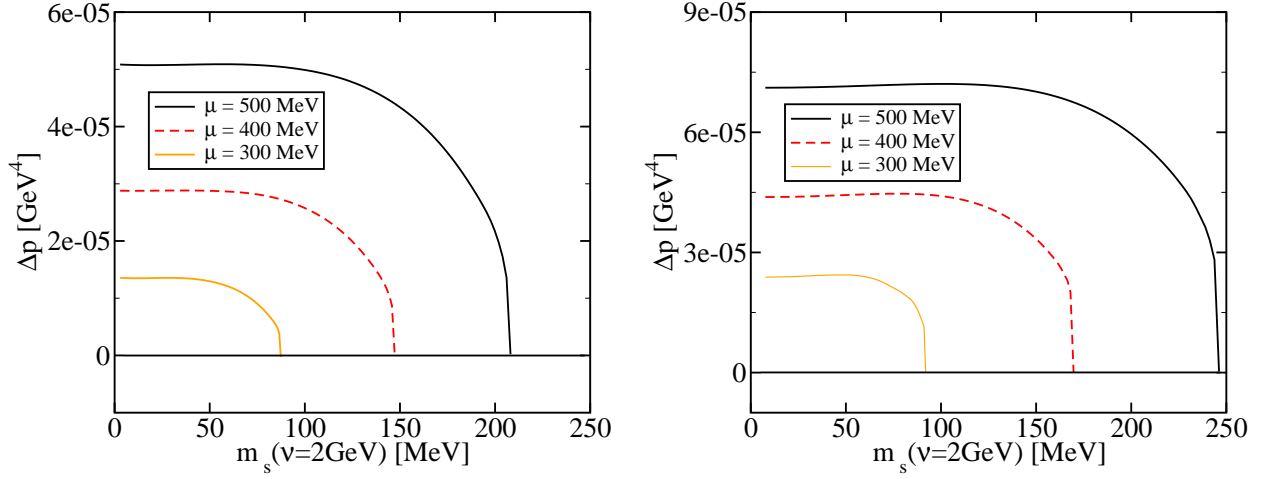


Figure 7: Pressure difference between 2SC and CFL phase as function of the renormalized strange quark mass at chemical potentials of $\mu = 300$ MeV, 400 MeV, 500 MeV for the coupling $\alpha_I(k^2)$ (left) and $\alpha_{II}(k^2)$ (right).

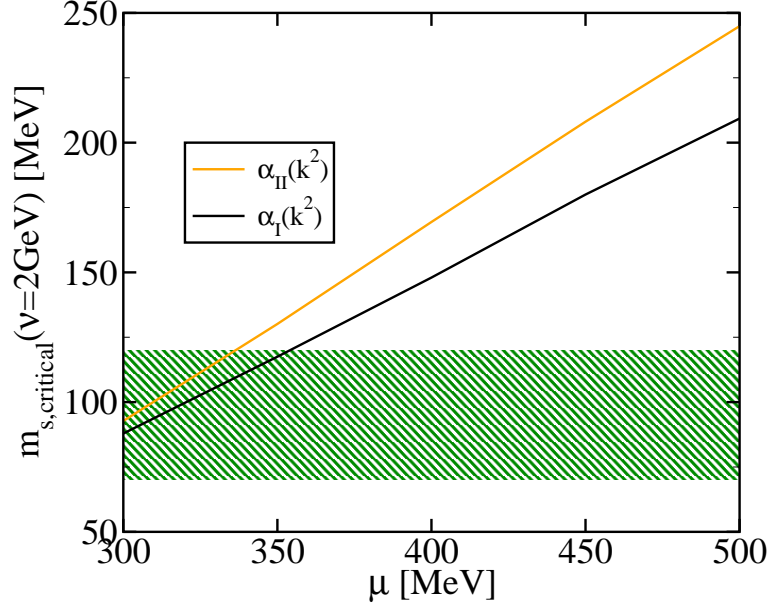


Figure 8: Critical renormalized strange-quark mass as a function of the chemical potential for the couplings $\alpha_I(k^2)$ and $\alpha_{II}(k^2)$ and the range stated by the particle data group [19] (shaded band).

potential for the physical value of the strange-quark current mass. This result is robust against variation of the running of the strong coupling in the infrared within the given uncertainties. Since the CFL phase is only mildly influenced by neutrality conditions we expect the result to hold even when neutrality is required. The critical value of the strange-quark current mass should then be similar or even slightly larger. This will be explored in further studies.

Given the present results a further investigation of the CFL phase by the inclusion of the Meissner effect and Goldstone-boson contributions is of interest since both are expected to decrease the gap functions. Also the temperature dependence and therefore the structure of the QCD phase diagram at large densities is within the reach of the type of investigations presented here.

- [11] D. Nickel, J. Wambach and R. Alkofer, Phys. Rev. D **73**, 114028 (2006) [arXiv:hep-ph/0603163].
- [12] C. S. Fischer and R. Alkofer, Phys. Rev. D **67**, 094020 (2003) [arXiv:hep-ph/0301094].
- [13] M. S. Bhagwat, M. A. Pichowsky, C. D. Roberts and P. C. Tandy, Phys. Rev. C **68**, 015203 (2003) [arXiv:nucl-th/0304003].
- [14] C. S. Fischer and M. R. Pennington, Phys. Rev. D **73**, 034029 (2006) [arXiv:hep-ph/0512233].
- [15] C. S. Fischer, P. Watson and W. Cassing, Phys. Rev. D **72**, 094025 (2005) [arXiv:hep-ph/0509213].
- [16] R. D. Pisarski and D. H. Rischke, Phys. Rev. D **60**, 094013 (1999) [arXiv:nucl-th/9903023].
- [17] Q. Wang and D. H. Rischke, Phys. Rev. D **65**, 054005 (2002) [arXiv:nucl-th/0110016].
- [18] D. Nickel, Annals Phys. in print, [arXiv:hep-ph/0607224].
- [19] W.-M. Yao *et al.*, J. Phys. G **33**, 1 (2006).
- [20] In addition, it is worth mentioning that solutions of the Bethe-Salpeter equation within the DSE approach in *MOM* scheme favor small values for the physical strange quark-current mass [15], a fact which is definitely related to the difference in renormalization schemes.
- [21] In principle, we also need to rescale μ , formally leading to two chemical potentials. This introduces no further complication in principle but is neglected for the sake of simplicity.